Journal Name

PAPER

A 1.5 mm BGO PET detector with DOI measurement

Siyuan Han[1], Xin Yu[1], Yibin Zhang[2], Lei Zhao[3], Liyan Zhao[2], Huiping Zhao[2], Jinyong Tao[2], Jianfeng Xu[1] and Qiyu Peng[2,*]

[1]School of Mechanical Science and Engineering, Huazhong University of Science and Technology

[2]Institute of Biomedical Engineering, Shenzhen Bay Laboratory, Shenzhen, People's Republic of China

[3]School of Electronics and Information Engineering, Harbin Institute of Technology

*Author to whom any correspondence should be addressed.

E-mail: qiyupeng@gmail.com

Keywords: DOI, light-sharing window, high-resolution detector

Abstract

To achieve a PET system that simultaneously offers high sensitivity, high spatial resolution, improved signal to noise ratio (SNR), and depth of interaction (DOI) measurement, we propose and implement a high DOI resolution PET detector based on a $1.5 \times 1.5 \times 20$ mm^3 BGO crystal array. In addition, we introduce a vertical line-source irradiation DOI calibration method, which enables simultaneous calibration of all detectors in the system and greatly simplifies the overall workflow. The proposed detector incorporates a 10×8 array of BGO crystals ($1.5 \times 1.5 \times 20$ mm^3) coupled to a 5×4 MPPC array. A 6 mm high light-sharing window (LSW) is placed between crystals to enhance the depth dependent light transport, thereby enabling effective DOI estimation even for low light yield BGO. DOI conversion functions were established using both mechanical collimation experiments and the proposed vertical line-source irradiation at the system center.

Using mechanical collimation, we obtained an average DOI resolution of 4.4 mm (FWHM) and a mean absolute error (MAE) of 2.2 mm at depths of 4, 8, 12, and 16 mm. With the vertical line-source irradiation method, the measured DOI resolution was 4.9 mm (FWHM) with an MAE of 3.1 mm. Imaging experiments using a Derenzo phantom demonstrated that DOI correction noticeably improved image sharpness and contrast. For the 1.1 mm rod structures, the valley to peak ratio (VPR) decreased from 60.7% (uncorrected) to 36.5% (mechanical collimation calibration) and 37.7% (vertical line-source irradiation calibration), confirming substantial enhancement in spatial resolution.

The proposed BGO detector and DOI calibration approach collectively provide high DOI performance, high sensitivity, and efficient calibration, offering a practical pathway toward the development of next generation high resolution and high sensitivity BGO based PET systems.

1 Introduction

Positron emission tomography (PET) is a key functional imaging modality in modern medical diagnostics [1, 2], and is widely used in oncology [3, 4], neuroscience [5], and cardiovascular studies [6, 7]. With the development of high resolution PET systems and large axial field of view (FOV) whole-body dynamic PET, increasingly stringent requirements have been placed on detector spatial resolution, sensitivity, and imaging uniformity. Increasing the length and packing fraction of scintillation crystals enhances the detector's ability to intercept γ-photons, thereby improving system sensitivity [8]. However, as illustrated in Fig. 1, longer crystals exacerbate the uncertainty of the γ photon depth of interaction (DOI), which in turn leads to parallax errors in the reconstructed line of response (LOR) [9, 10]. Therefore, DOI measurement play a crucial role in mitigating parallax error and improving the uniformity of spatial resolution across the imaging field of view.

Scintillation crystals are a key determinant of PET detector performance [11]. Although LYSO has received considerable attention in recent years due to its high light yield and fast decay time [12], BGO continues to exhibit irreplaceable advantages in certain PET system designs . First, BGO has a high density (7.13 g/cm^3) and a high effective atomic number, providing excellent stopping power for 511 keV photons [13], and enabling the construction of PET detectors with
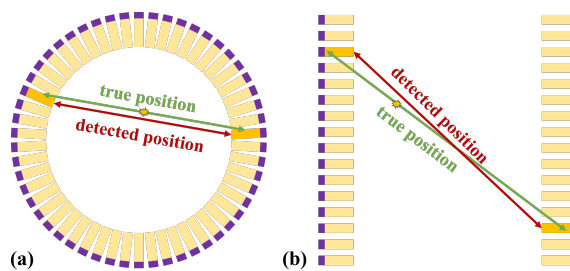
Figure 1. Illustration of DOI-induced LOR parallax. (a) Parallax effect in the transverse direction; (b) Parallax effect in the axial direction.

higher sensitivity. Second, unlike LYSO, BGO contains no radioactive isotope such as ^{176}Lu, resulting in extremely low intrinsic background radiation. This characteristic makes BGO particularly suitable for low activity, low dose, and ultra high sensitivity PET systems, such as high sensitivity small animal PET [14]. Third, BGO is relatively inexpensive, industrially mature, and can be mass produced in large sizes [15], making it an attractive option for building ultra long axial field of view PET systems, such as total body PET.

However, compared with LYSO, BGO exhibits clear disadvantages in optical performance, most notably its lower light output and longer decay time. In previous studies, Kratochwil *et al.* [16] developed a PET detector using $2 \times 2 \times 3$ mm^3 BGO crystals and achieved high system sensitivity; however, the design lacked DOI measurement. Gonzalez-Montoro *et al.* [17] employed a monolithic $50 \times 50 \times 15$ mm^3 BGO crystal and obtained a DOI resolution of 5 mm, but the decoding accuracy was susceptible to crystal non-uniformity and edge effects. Inadama *et al.* [18] implemented a four layer BGO detector composed of $2.9 \times 2.9 \times 7.5$ mm^3 crystals and achieved discrete DOI estimation; however, this multilayer structure required precise layer by layer alignment, increasing fabrication complexity and cost. Therefore, developing a BGO based PET detector that simultaneously achieves high spatial resolution and DOI measurement remains a significant challenge [19].

In this study, we propose and realize a BGO based PET detector with high DOI resolution. Through optical structural optimization, we achieve an average DOI resolution of 4.4 mm (FWHM) and a mean absolute error (MAE) of 2.2 mm using crystals of size $1.5 \times 1.5 \times 20$ mm^3. Moreover, we introduce a rapid DOI calibration method based on vertical line-source irradiation, which enables calibration of the entire detector array in a single measurement. This method yields DOI performance comparable to the mechanically collimated reference experiment, with a resolution of 4.9 mm and an MAE of 3.1 mm. Imaging experiments using a Derenzo phantom demonstrate that DOI correction substantially improves spatial resolution: the valley to peak ratio (VPR) for the 1.1 mm rod structures decreased from 60.7% (uncorrected) to 36.5% (mechanical collimation calibration) and 37.7% (vertical line-source irradiation calibration), confirming the effectiveness of the proposed detector in improving image clarity and spatial resolution.

2   Methods and materials

2.1   Detector design

The detector consists of a BGO crystal array optically coupled to a multi- pixel photon counter (MPPC) array using optical grease (BC-630, refractive index 1.4). The BGO array is arranged in a 10×8 matrix, with each crystal pixel measuring $1.5 \times 1.5 \times 20$ mm^3. The MPPC array is configured as a 5×4 matrix, with each MPPC element having an active area of 3×3 mm^2. Light-sharing windows (LSWs) made of the same optical grease (BC-630) are inserted between adjacent crystals. Each LSW has a height of 6 mm and partially transmits scintillation light according to the DOI, as illustrated in Fig. 2. This structural design enhances depth dependent light transport and enables DOI measurement. The output signals from the MPPC array are read out through a 1-bit delta-sigma circuit [20].

2.2   Mechanical collimation calibration

To evaluate the DOI measurement performance of the BGO detector, a mechanical collimation experiment was conducted. As shown in Fig. 3, a tungsten collimator was positioned adjacent to one side of the detector. The collimator had a thickness of 45 mm, a slit width of 2 mm, and a slit length of 40 mm. On the opposite side of the collimator, a line-source phantom was placed. The line source had a diameter of 2 mm and a length of 40 mm, and was filled with a uniform ^{18}F-FDG
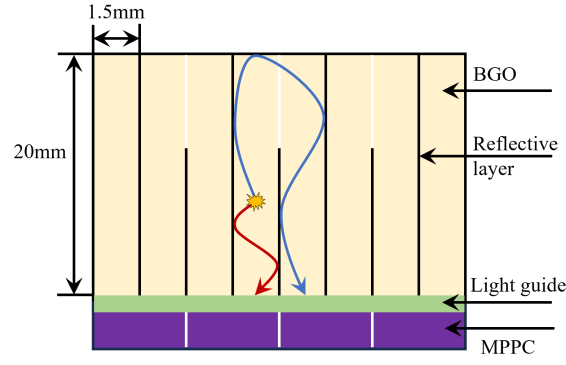
Figure 2. A schematic diagram of the LSW is shown in the figure. As the DOI increases, the number of scintillation photons propagating along the red path and reaching the first MPPC gradually decreases, while the number of photons traveling along the blue path and reaching the other MPPC correspondingly increases. The DOI can therefore be calculated based on the difference between the signals generated by the two MPPCs.
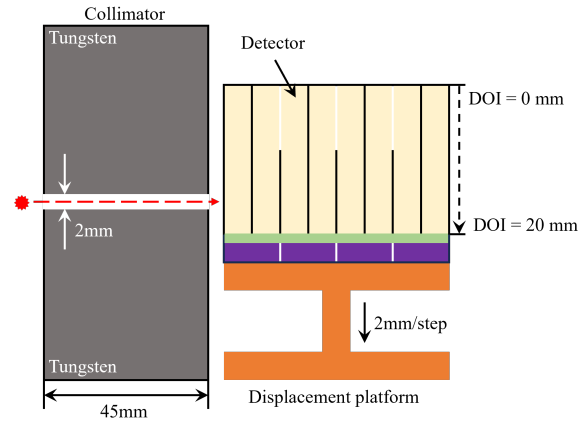

Figure 3. Schematic of the mechanical collimation experiment. A tungsten slit (width 2 mm, thickness 45 mm) collimates the line source. The collimated beam is stepped along the crystal depth from 2 mm to 18 mm in 2 mm increments, corresponding to the DOI positions used in calibration and evaluation.

solution with an initial activity of 7.4 MBq.

A single detector module was used, and the collimator was translated in 2 mm increments to acquire count-rate data at depths ranging from 2 mm to 18 mm. For each depth position, one million events were recorded. An energy window of ± 100 keV was applied to reject scattered events. Data acquired at depths of 2, 6, 10, 14, and 18 mm were used to fit the DOI conversion function, whereas data obtained at 4, 8, 12, and 16 mm were used to determine the intrinsic DOI resolution of the detector. Subsequently, the vertical line-source irradiation calibration method was applied to validate the DOI resolution. The system performance was evaluated using the full width at half maximum (FWHM) and the mean absolute error (MAE) derived from the DOI measurements.

2.3 Vertical line-source irradiation calibration

In PET systems, performing mechanical collimation and scanning on each detector module individually is a time-consuming and labor-intensive calibration procedure. Such an approach is impractical for real-world applications, especially for rapid calibration of large detector arrays. To address this limitation, we designed and implemented an efficient line-source calibration method aimed at achieving fast and global DOI calibration.

In this method, a line shaped radioactive source filled with ^{18}F-FDG is placed at the geometric center of the PET scanner. Under this configuration, the incident γ-photons can be regarded as impinging perpendicularly onto the front face of every detector module surrounding the source. When a 511 keV γ-ray enters a BGO crystal of thickness H at normal incidence, the probability density that the photon interacts at a depth h follows an exponential attenuation model. The normalized depth-response function $C(h)$ can be expressed as:

$$C(h) = \frac{C_{\text{Total}}}{1 - e^{-\mu H}}\, \mu e^{-\mu h}, \quad 0 \le h \le H, \tag{1}$$
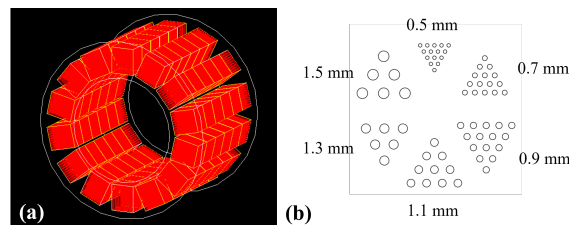
Figure 4. (a) Schematic diagram of the BGO-based PET system, which has an axial length of 88.3 mm and a bore diameter of 85.48 mm. (b) Derenzo phantom used in the simulation, featuring rod diameters of 0.5, 0.7, 0.9, 1.1, 1.3, and 1.5 mm.

where C_{Total} is the total number of detected events, μ (cm^{-1}) is the linear attenuation coefficient of BGO for the incident gamma-ray energy, and h is the interaction depth measured from the crystal surface.

This model is derived from the Beer–Lambert law and represents the depth-dependent probability density of photon interactions within a scintillator of finite thickness [21]. The normalization term $(1 - e^{-\mu H})$ ensures that the integral of $C(h)$ over the range $[0, H]$ equals C_{Total}. In the case of 511 keV photons, μ for BGO is approximately 0.96 cm^{-1}, corresponding to an attenuation length of about 10.4 mm [22].This exponential attenuation model provides a theoretical foundation for DOI calibration, as fitting the experimentally measured data to this distribution enables the mapping of the detected light signals to the corresponding depths of interaction.

2.4 Derenzo phantom imaging

A GATE simulation was performed using the same BGO detector configuration to validate the performance of the vertical line-source irradiation DOI calibration method. GATE (Geant4 Application for Tomographic Emission) is a Monte Carlo simulation platform based on Geant4 and is widely used for modeling the physical processes in nuclear medicine imaging systems [23]. It accurately simulates detector response, photon transport, electronic processes, and system geometry.

In this study, the PET system consisted of 14 panels, each containing a 1×6 array of detector modules with a physical size of 17.8 mm $\times$ 88.3 mm. The resulting system had an axial length of 88.3 mm and a bore diameter of 85.48 mm, as depicted in Fig. 4(a). The energy resolution was set to 18% at 511 keV, with an energy window of ± 150 keV, and a coincidence time window of 5 ns.

To assess the imaging performance, a Derenzo phantom was placed at the center of the system. Fig. 4(b) shows the configuration of the phantom, which contains rods with diameters of 0.5, 0.7, 0.9, 1.1, 1.3, and 1.5 mm, and has an overall thickness of 90 mm. The phantom was filled with 2.5 MBq of ^{18}F-FDG, and data were acquired for 30 min. Image reconstruction was performed using the 3D-OSEM algorithm with a matrix size of $450 \times 450 \times 450$ and a voxel size of $0.2 \times 0.2 \times 0.2$ mm^3. The reconstruction parameters included 4 subsets and 10 iterations.

3 Results and analysis

3.1 Flood maps

Fig. 5(a) shows the flood map obtained from the BGO crystal array under vertical line-source irradiation. Because the system employs a single-ended DOI readout configuration, variations in the DOI affect the distribution of scintillation light among the MPPC channels. This, in turn, alters the relative signal ratios used in the centroid algorithm and results in position shifts, leading to a flood-map pattern that differs from traditional crystal identification maps.

Figs. 5(b)–(e) display the flood maps of four crystals located on the same MPPC channel but interacting at different DOI depths of 4, 8, 12, and 16 mm, respectively. As the DOI varies, the relative light-sharing ratios among MPPC channels change significantly, causing noticeable positional shifts when event coordinates are computed using the centroid method. These flood maps provide an intuitive visualization of how the spatial distribution of scintillation photons evolves with DOI within the detector.

As the interaction depth increases from 4 mm to 16 mm, the centroid of the flood-map distribution gradually shifts away from the region of the LSW. Specifically, in Fig. 5(b), the bright spots appear relatively dispersed, whereas in Fig. 5(c) they begin to cluster, indicating a reduced fraction of scintillation photons transmitted through the LSW. In Fig. 5(d), the bright spots become more concentrated and exhibit a pronounced positional shift.
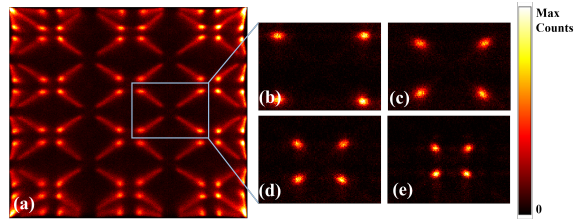
Figure 5. (a) Flood map obtained from the vertical line-source irradiation of the BGO crystal, (b)–(e) Flood maps of 4 mm, 8 mm, 12 mm, and 16 mm, respectively.
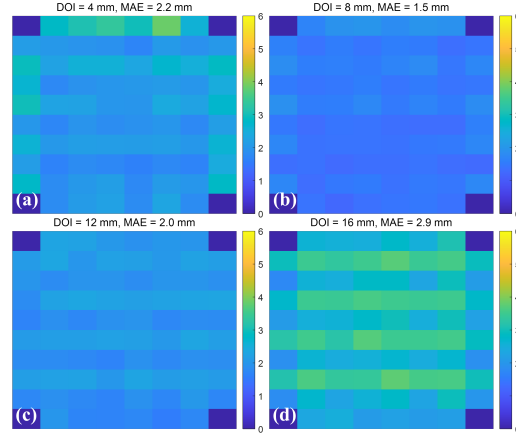

Figure 6. (a)-(d) Presents the MAEs obtained from the mechanical collimation experiment at DOI depths of 4 mm, 8 mm, 12 mm, and 16 mm.

This behavior can be attributed to the increasing depth of interaction, which reduces the angular spread of scintillation photons reaching the LSW. As a result, the probability that photons traverse the LSW and reach neighboring MPPC elements decreases. This effect is clearly illustrated in Fig. 5, where the reconstructed crystal positions in the flood maps progressively shift farther from the LSW as the depth increases from 4 mm to 16 mm.

3.2   DOI resolution

Fig. 6 presents the DOI measurement results obtained from the mechanical collimation experiment. Data acquired at depths of 2, 6, 10, 14, and 18 mm were used to fit the DOI conversion function, while data from 4, 8, 12, and 16 mm were used to calculate the intrinsic DOI resolution of the detector. The MAEs for these depths were 2.2 mm, 1.5 mm, 2.0 mm, and 2.9 mm, respectively, and the average FWHM over all depths was 4.4 mm. This method provides an estimate of the intrinsic
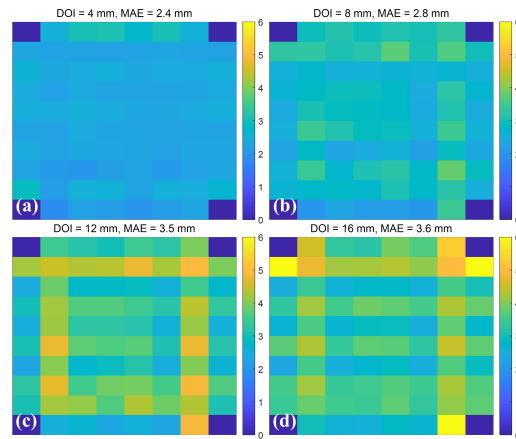

Figure 7. (a)-(d) Presents the MAEs obtained from the vertical line-source irradiation calibration of the BGO crystals at DOI depths of 4 mm, 8 mm, 12 mm, and 16 mm.
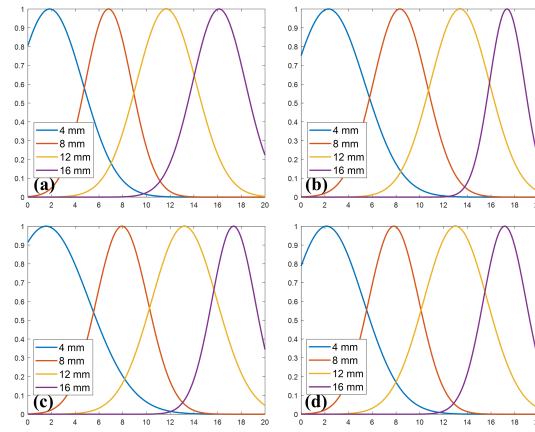
Figure 8. The DOI spectrum of the selected crystals.

DOI resolution achievable by the detector under the experimental conditions. The obtained results were subsequently compared with the DOI calibration derived from the vertical line-source irradiation experiment to further validate the accuracy of the proposed approach.

Fig. 7 shows the DOI calibration results obtained using the vertical line-source irradiation method. At interaction depths of 4, 8, 12, and 16 mm, the MAEs were 2.4 mm, 2.8 mm, 3.5 mm, and 3.6 mm, respectively, with an average FWHM of 4.9 mm across all depths. Compared with the intrinsic DOI resolution obtained via mechanical collimation in Fig. 6, the performance of the vertical line-source irradiation calibration method is slightly degraded, as expected. Fig. 8 further illustrates Gaussian fits of the DOI distributions for four randomly selected crystals under different collimated depth positions, obtained using the vertical line-source irradiation method.

3.3   Derenzo phantom imaging

Fig. 9(a) shows the reconstructed slice of the Derenzo phantom without DOI correction, while Fig. 9(b) and Fig. 9(c) present slices at the same axial position after applying DOI correction using the mechanical collimation calibration method and the vertical line-source irradiation calibration method, respectively. Fig. 9(d) shows the corresponding line profiles extracted along the 1.1 mm rod structures, which were used to compute the VPR.

After DOI correction, the rod structures particularly the smaller ones become more clearly resolved. This enhancement arises from the improved DOI resolution, which effectively reduces parallax error and increases the accuracy of localizing the γ-photon interaction positions. In contrast, the image reconstructed without DOI correction exhibits pronounced blurring and reduced contrast, primarily due to parallax artifacts caused by the absence of depth information. Both DOI calibration methods successfully provide accurate interaction-depth information, leading to significantly improved image quality and demonstrating the strong potential of the proposed detector design for high spatial resolution PET imaging.

As shown in Fig. 9(d), the VPR of the 1.1 mm rod structures in the central region is 60.7% without DOI correction. After applying DOI correction using the mechanical collimation method, the VPR decreases to 36.5%, while the vertical line-source irradiation method yields a VPR of 37.7%. The VPR reflects the system's ability to resolve rod structures of a given diameter, with a lower value indicating higher spatial resolution. In this study, spatial resolution is evaluated using the VPR metric, and a commonly accepted criterion is that a structure can be clearly resolved when its VPR is below 0.735. The reconstructed images obtained with both DOI calibration methods satisfy this criterion and achieve a spatial resolution of approximately 1.1 mm, demonstrating comparable performance.

4   Discussion

Using vertical line-source irradiation of the BGO crystals, we achieved a fast and accurate DOI calibration method for PET detectors, the DOI resolution was 4.9 mm (FWHM) with an MAE of 3.1 mm for all crystals. When applied to the PET system, this calibration method significantly improved the reconstructed image quality and spatial resolution, achieving a resolution of 1.1 mm.

Using mechanical collimation for DOI calibration, the DOI resolution for all crystals was 4.4 mm, with an MAE of 2.2 mm. Although the DOI resolution obtained using vertical line-source
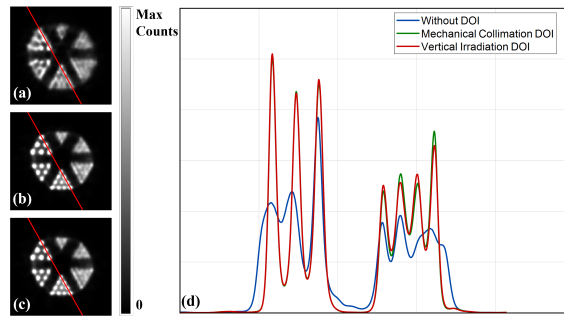
Figure 9. (a) Reconstructed slice of the Derenzo phantom without DOI correction; (b) reconstructed slice after applying DOI calibration using the mechanical collimation method; (c) reconstructed slice after applying DOI calibration using the vertical line-source irradiation method; (d) corresponding line profiles extracted from the three reconstructed images.

irradiation is slightly lower than that obtained with mechanical collimation, its primary advantages lie in efficiency and simplicity. Only 600 s of data acquisition are required for each detector to collect sufficient statistics for DOI calibration, without the need for collimation hardware. This method enables simultaneous calibration of all detector modules in the system and avoids disassembly or dedicated collimator fabrication, greatly simplifying the calibration workflow and facilitating system upgrades.

However, the method also has certain limitations. Under vertical line-source irradiation, it is difficult to guarantee perfect perpendicular alignment for every crystal, particularly those located at the detector edges. In addition, the exponential attenuation model used for BGO crystal irradiation is an idealized representation. The Beer–Lambert law only describes the unscattered attenuation path, while scattering, interface reflections, and other optical effects also occur in practice. Therefore, using a single attenuation coefficient μ as the prior parameter cannot fully account for these factors.

Another source of error arises from the event-distribution characteristics under vertical line-source irradiation. As shown in Fig. 5(a), the interaction events exhibit an elongated distribution along a diagonal direction in the detector plane. Consequently, in Fig. 7, a noticeable discrepancy appears between the outermost crystal ring and the second-to-outermost ring as the DOI increases. This effect occurs because the elongated event clusters near the detector edges may cause events that should belong to the second ring to be incorrectly assigned to the outer ring (or vice versa), making crystal discrimination more challenging. By contrast, the mechanical collimation method constrains the incident angle, producing a more concentrated response distribution (without diagonal elongation), and thus no such systematic edge deviation is observed in Fig. 6.

Additionally, several factors influence the achievable DOI resolution. The probability that scintillation photons propagate through the LSWs and reach neighboring MPPC elements varies with DOI depth, leading to depth-dependent differences in the detected energy. Therefore, applying a fixed energy window for events across all DOI depths is not optimal. The results presented in this study were obtained using a uniform ± 100 keV energy window, which may not be ideal and warrants further investigation.

Several approaches may further improve the DOI resolution of the vertical line-source irradiation calibration method. First, optimizing the packaging and assembly of the BGO crystal array could reduce non-uniformities caused by scintillation light transport losses, thereby improving overall detector uniformity and performance. In addition, while this study employed a uniform ± 100 keV energy window for event selection, future work will explore depth dependent energy windows potentially determined through iterative optimization to further enhance calibration accuracy and overall system performance.

5   Conclusion

In this study, we proposed and implemented a high-DOI-resolution PET detector based on BGO crystals. By introducing LSWs between crystals and optimizing the optical design, we achieved effective depth sensitivity within BGO crystals of only 1.5 mm in width, demonstrating the feasibility of accurate DOI measurement using BGO. In parallel, we developed a vertical line-source irradiation calibration method that eliminates the need for mechanical collimation, enabling rapid DOI calibration without detector disassembly and significantly reducing system complexity and

associated costs.

Experimental results show that the proposed line-source calibration strategy achieved an average DOI resolution of approximately 4.9 mm (FWHM) across all crystals. Although slightly inferior to the 4.4 mm obtained using mechanical collimation, the performance is sufficient to support effective DOI correction. In imaging experiments, the DOI information obtained from this method markedly improved reconstruction quality, enhancing the visibility of fine structures in the Derenzo phantom. Notably, the VPR of the 1.1 mm rods decreased from 60.7% (uncorrected) to 37.7%, confirming the substantial improvement in spatial resolution.

Despite its clear advantages in efficiency and ease of use, the line-source calibration method is affected by several limitations. Its performance depends strongly on the uniformity of the detector's internal optical coupling, and any non-uniformity in crystal response or optical bonding can degrade the accuracy of the DOI conversion function. Furthermore, perfect geometric alignment during vertical line-source irradiation cannot be guaranteed for all crystals, particularly those at the detector edges. The exponential attenuation model employed is also an approximation, as it does not account for more complex phenomena such as scattering and interface reflections.

The proposed vertical line-source irradiation DOI calibration method thus offers key advantages by greatly simplifying the calibration workflow; however, it remains partially constrained by these practical and modeling limitations. Future work will focus on addressing these issues to further improve the robustness and general applicability of the method. Potential improvements include refining the crystal-array packaging process to reduce light-transport non-uniformities and implementing depth-dependent or iteratively optimized energy windows to enhance calibration accuracy.

In conclusion, this study demonstrates a viable DOI-capable PET detector architecture based on BGO crystals and validates its effectiveness in improving imaging uniformity and spatial resolution. The proposed approach provides a practical technological foundation for developing next-generation, high-sensitivity PET systems that leverage BGO scintillators while incorporating DOI capability.

Author contributions
Siyuan Han: Data curation, Formal analysis, Investigation, Visualization, Writing. Xin Yu: Methodology, Detector design, Investigation. Yibin Zhang: Funding acquisition, Project administration. Lei Zhao: Software, GATE simulation, Validation. Liyan Zhao: Investigation, Experimental measurements. Huiping Zhao: Hardware design, Electronics system development. Jinyong Tao: Firmware development, Software support. Jianfeng Xu: Supervision, Project administration. Qiyu Peng: Conceptualization, Supervision, Project administration.

References
[1] Muehllehner G and Karp J S 2006 *Physics in Medicine & Biology* **51** R117

[2] Bailey D L, Maisey M N, Townsend D W and Valk P E 2005 *Positron emission tomography* vol 2 (Springer)

[3] Enghardt W, Crespo P, Fiedler F, Hinz R, Parodi K, Pawelke J and Poenisch F 2004 *Nuclear Instruments and Methods in Physics Research Section A: Accelerators, Spectrometers, Detectors and Associated Equipment* **525** 284–288

[4] Schöder H and Gönen M 2007 *Journal of Nuclear Medicine* **48** 4S–18S

[5] Nordberg A, Rinne J O, Kadir A and Långström B 2010 *Nature Reviews Neurology* **6** 78–87

[6] Bengel F M and Schwaiger M 2004 *Journal of nuclear cardiology* **11** 603–616

[7] Kolbitsch C, Ahlman M A, Davies-Venn C, Evers R, Hansen M, Peressutti D, Marsden P, Kellman P, Bluemke D A and Schaeffter T 2017 *Journal of nuclear medicine* **58** 846–852

[8] Xu J, Xie S, Zhang X, Tao W, Yang J, Zhao Z, Weng F, Huang Q, Yi F and Peng Q 2019 *Physics in Medicine & Biology* **64** 155009

[9] Watanabe M, Moriya T, Uchida H and Omura T 2021 *Physics in Medicine & Biology* **66** 18NT02

[10] Cabello J, Etxebeste A, Llosá G and Ziegler S I 2015 *Physics in Medicine & Biology* **60** 3673

[11] Lewellen T K 2008 *Physics in Medicine & Biology* **53** R287

[12] Alva-Sánchez H, Zepeda-Barrios A, Díaz-Martínez V, Murrieta-Rodríguez T, Martínez-Dávalos A and Rodríguez-Villafuerte M 2018 *Scientific reports* **8** 17310

[13] Yu X, Zhang X, Zhang H, Peng H, Ren Q, Xu J, Peng Q and Xie S 2022 *Crystals* **12** 1302

[14] Du J, Ariño-Estrada G, Bai X and Cherry S R 2020 *Physics in Medicine & Biology* **65** 235030

[15] Gonzalez-Montoro A, Pourashraf S, Cates J W and Levin C S 2022 *Frontiers in Physics* **10** 816384

[16] Kratochwil N, Auffray E and Gundacker S 2020 *IEEE Transactions on Radiation and Plasma Medical Sciences* **5** 619–629

[17] Gonzalez-Montoro A, Sanchez F, Majewski S, Zanettini S, Benlloch J and Gonzalez A 2017 *Journal of Instrumentation* **12** C11027

[18] Inadama N, Murayama H, Yamaya T, Kitamura K, Yamashita T, Kawai H, Tsuda T, Sato M, Ono Y and Hamamoto M 2006 *IEEE transactions on nuclear science* **53** 30–34

[19] Miyaoka R, Lewellen T, Yu H and McDaniel D 1998 *IEEE Transactions on Nuclear Science* **45** 1069–1073

[20] Cheng X, Hu K and Shao Y 2019 *IEEE transactions on nuclear science* **66** 2107–2113

[21] Knoll G F 2010 *Radiation detection and measurement* (John Wiley & Sons)

[22] Enríquez-Mier-y Terán F E, Ortega-Galindo A S, Murrieta-Rodríguez T, Rodríguez-Villafuerte M, Martínez-Dávalos A and Alva-Sánchez H 2020 *EJNMMI physics* **7** 21

[23] Jan S, Santin G, Strul D, Staelens S, Assié K, Autret D, Avner S, Barbier R, Bardies M, Bloomfield P *et al.* 2004 *Physics in Medicine & Biology* **49** 4543